Available online at www.sciencedirect.com
SCIENCE DIRECT®
International Journal of Thermal Sciences 44 (2005) 1039–1046
International Journal of Thermal Sciences
www.elsevier.com/locate/ijts

Numerical simulation of capillary plasma flow generated by high-current pulsed power

Kyoungjin Kim *

Department of Mechanical Engineering, The University of Texas at Austin, 1 University Station, Mail Code C2200, Austin, TX 78712, USA

Received 20 April 2004; received in revised form 12 April 2005; accepted 14 April 2005

Available online 31 May 2005

Abstract

Pulsed plasma discharge in the interior region of electrothermal–chemical gun is numerically investigated with the one-dimensional time-dependent mathematical modeling that includes the Joule heating of plasma column and the mass ablation of bore wall. Sonic boundary condition is utilized because flow is expected to be choked at the bore exit. In the evaluation of thermodynamic and transport properties, plasma state is assumed to be in local thermal equilibrium due to high pressure and is found to be weakly nonideal. The computational results show that capillary plasma flow at the bore exit is partially ionized high temperature and high pressure discharge. Many predicted data including arc resistance, energy deposition, and bore wall mass ablation are favorably compared with the measurements on total 8 shots of gun firings with different levels of energy deposition ranging from 5.3 to 47 kJ. Temporal evolution of pressure shows transient effect in the calculations but the effect is minimal compared to the significant transient effect in the pressure measurements. However, maximum pressure is in good agreement with measured data.

Keywords: Capillary plasma flow; Electrothermal–chemical gun; Pulsed power

1. Introduction

An electrothermal–chemical (ETC) gun is the device for producing a pulsed plasma discharge using high-magnitude current pulses. The process employs a high-power discharge of electrical energy to vaporize the solid materials of capillary bore (typically polycarbonate or polyethylene), and the eroded vapor is subsequently ionized to form a dense plasma flow during the duration of a high current discharge. The vapor plasma then exits the open end of the bore to create a high-velocity, high-temperature, and high-pressure external plasma jet into the background gas in an open or closed chamber. This technology has been originally developed to improve the combustion rate of the solid propellants as an alternative to the conventional chemical igniters for the acceleration of projectiles [1]. Also, this concept can be used for producing metal vapor plasmas for the synthesis of novel ceramic and metal nanocrystalline materials or the other material processing applications by utilizing the extreme conditions of plasma discharge [2].

There have been several different approaches of numerical simulation depending on the degree of modeling simplification. By neglecting the axial dependence of temperature and pressure and adopting volume-averaged properties, Mohanti and Gilligan [3] established time-dependent zero-dimensional model. Powell and Zielinski [4] introduced a simple quasi-steady isothermal model and it provides reasonable predictions despite its simplicity. Raja et al. [5] assumed that the plasma flow is quasi-steady in their one-dimensional modeling of the electrogun and considered the electrode erosion based on Langmuir relationship as well as the bore wall ablation. Powell and Zielinski [6], Zoler and Alimi [7], and Zaghloul et al. [8] carried out more sophisticated theoretical analysis using the time-dependent one-dimensional models.

* Phone: +1 512 471 3137; fax: +1 512 471 1045.
E-mail address: kimkj@mail.utexas.edu (K. Kim).

1290-0729/$ – see front matter
doi:10.1016/j.ijthermalsci.2005.04.007

Nomenclature

c_s	speed of sound	$\mathrm{m\cdot s^{-1}}$
e	specific internal energy	$\mathrm{J\cdot kg^{-1}}$
e_c	electron charge	C
f	deviation factor from blackbody radiation heating	
h	Planck constant	J·s
I_i	ionization energy of heavy species i	J
J	current density	$\mathrm{A\cdot m^{-2}}$
k	Boltzmann constant	$\mathrm{J\cdot K^{-1}}$
L	bore length	m
$\bar{m}$	average particle mass of heavy species	kg
m_e	electron mass	kg
n	number density	$\mathrm{m^{-3}}$
P	pressure	Pa
Q_i	partition function of heavy species i	
R_h	average gas constant of heavy species	$\mathrm{J\cdot kg^{-1}\cdot K^{-1}}$
r_b	bore radius	m
T	temperature	K
t	time	s
u_z	axial velocity	$\mathrm{m\cdot s^{-1}}$
z	axial coordinate	m

Greek symbols

α	degree of ionization	
ΔI_i	nonideal plasma correction to the ionization energy of heavy species	J
ε_0	vacuum permittivity	$\mathrm{F\cdot m^{-1}}$
γ	plasma nonideality parameter	
γ_{eff}	effective specific heat ratio	
ρ	total plasma mass density	$\mathrm{kg\cdot m^{-3}}$
ρ_p	polyethylene plasma mass density	$\mathrm{kg\cdot m^{-3}}$
$\dot{\rho}_a$	mass ablation density rate	$\mathrm{kg\cdot m^{-3}\cdot s^{-1}}$
σ	plasma electrical conductivity	$\mathrm{S\cdot m^{-1}}$
σ_{sb}	Stefan–Boltzmann constant	$\mathrm{W\cdot m^{-2}\cdot K^{-4}}$
$\bar{\nu}_{ei}$	electron–ion momentum transfer collision frequency	$\mathrm{s^{-1}}$
$\bar{\nu}_{en}$	electron–neutral momentum transfer collision frequency	$\mathrm{s^{-1}}$

Subscripts

i	heavy species i
ion	ion
e	electron

In the present work, the numerical simulation of the plasma discharge in the ETC gun is performed by utilizing the time-dependent one-dimensional gas dynamics equations. The computational results are compared with the extensive measurements of total eight cases of ETC gun firing with different levels of energy deposition, which were carried out by Powell and Zielinski [4].

2. Numerical modeling of plasma discharge

2.1. Electrothermal–chemical gun

A schematic diagram of the ETC gun is shown in Fig. 1 with the description of plasma discharge mechanism. The ETC gun is driven by a pulse-forming network (PFN), which consists of the capacitor banks, inductors, resistors, and ignition switch. In the experimental investigations by Powell and Zielinski [4], the capillary bore is made of polyethylene (CH_2) with a large aspect ratio of bore length to bore diameter.

Available experimental conditions and measured data for total eight firings are summarized in Table 1. Deposited energy in the plasma capillary ranges from 5.3 to 47.0 kJ, and the peak arc current varies from 7.5 to 58.7 kA. After each firing, the bore was drilled into larger diameter, as listed in the table. In the present calculations, the initial bore radius before the firing was used for each shot as specified in Table 1. Alternatively, the average radius might be used or even the use of variable bore radius might be a better approach in the computations, but its effect turned out to be minimal due to small change of bore radius after each firing. Bore size was not provided for shots 1 and 3, so the bore radius is linearly extrapolated based on the deposited energy and the bore radii used in the present analysis are 3.107 and 3.270 mm for shots 1 and 3, respectively. Note that the bore length is 60.9 mm for all the shots.

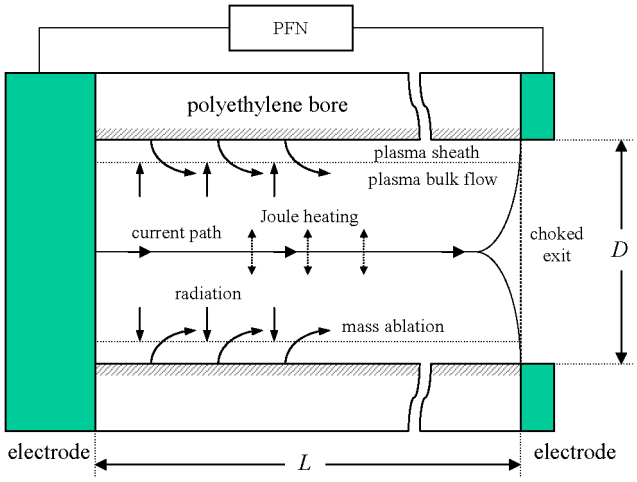

Fig. 1. Schematic diagram of electrothermal–chemical gun.

Fig. 2 shows the experimentally recorded trace of plasma arc current during the gun firing for shot 8. The peak current of approximately 47 kA was obtained at the time of approximately 450 μs, and the entire pulse duration of the electrical discharge is approximately 850 μs.

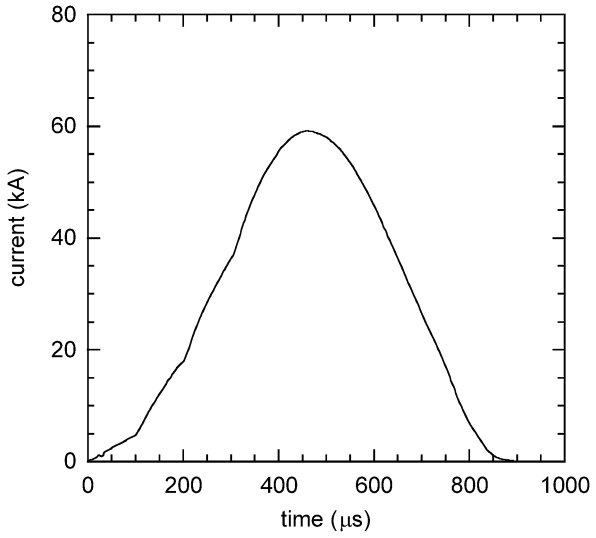

Fig. 2. Measured electrical current across the capillary bore for shot 8 with the deposited energy of 47 kJ [4].

Table 1
Summary of measurement data by Powell and Zielinski [4]

Shot number	maximum current (kA)	deposited energy (kJ)	initial bore radius (mm)	final bore radius (mm)	ablated mass (mg)
1	7.50	5.3	*	*	23.4
2	10.5	7.3	3.175	*	32.3
3	23.8	15.0	*	3.302	66.9
4	31.9	21.4	3.365	3.454	109.7
5	41.9	29.8	3.454	3.543	113.2
6	45.3	34.1	3.568	3.670	133.5
7	47.4	37.4	3.683	3.797	155.0
8	58.7	47.0	3.835	3.962	180.0

* Not measured.

2.2. Mathematical model of plasma discharge

A brief illustration of the plasma discharge dynamics is shown in Fig. 1. When the discharge of stored electrical energy from the capacitor banks is initiated, a fuse wire across the capillary bore explodes and provides an initial current path for the discharge. The mass ablation from the bore wall is mainly due to the radiative energy transport from the bulk plasma flow. Ablated bore material is entrained to the bulk plasma flow, which is subject to the intense Joule heating, and subsequently heated and ionized. Due to the large aspect ratio of bore length to the bore diameter, which is typical in ETC gun operations, axial transport of mass, momentum, and energy is expected to be dominant, compared to the radial transport, and it is a reasonable approximation that the plasma flow properties are fairly uniform over the cross section of the bore, except for the extremely thin vapor boundary layer near the bore wall. Therefore, by following the radial averaging over the bore cross section [4], the one-dimensional form of time-dependent governing equations for the conservation of mass (total and polyethylene component), momentum (in axial direction), and energy is given by

$$\frac{\partial \rho}{\partial t} + \frac{\partial}{\partial z}(\rho u_z) = \dot{\rho}_a \tag{1}$$

$$\frac{\partial \rho_p}{\partial t} + \frac{\partial}{\partial z}(\rho_p u_z) = \dot{\rho}_a \tag{2}$$

$$\frac{\partial \rho u_z}{\partial t} + \frac{\partial}{\partial z}\left(\rho u_z^2\right) = -\frac{\partial P}{\partial z} \tag{3}$$

$$\frac{\partial \rho \varepsilon}{\partial t} + \frac{\partial}{\partial z}\left(\rho u_z\left(\varepsilon + \frac{P}{\rho}\right)\right) = \frac{J^2}{\sigma} \tag{4}$$

$$\varepsilon = e + \frac{u_z^2}{2} \tag{5}$$

These equations represent the inviscid compressible gas dynamics in axial direction. In the energy transport equation, J^2/σ presents the Joule heating in the plasma column and the current density is also assumed to be uniform in the bore.

In order to model the mass ablation from the bore wall due to radiative heating, mass ablation density rate $\dot{\rho}_a$ is introduced in the mass transport equations as a source term, and the mass ablation can be approximated by equating the radiative flux from the plasma to the interior wall of the capillary bore and the energy flux of the ablated material inside the bore [6,7]. Thus, $\dot{\rho}_a$ is determined by

$$\dot{\rho}_a = \frac{2 f \sigma_{\mathrm{sb}} T^4 / r_b}{\varepsilon + P/\rho} \tag{6}$$

where the factor f represents the deviation of radiative heating from the blackbody behavior. In the previous computational work [9] for the operation of 3 kJ small-scale plasma capillary device with polycarbonate bore [10], deviation factor of 0.85 yielded good agreement with the measured mass loss of the bore, and this value of 0.85 is kept constant for all the shots in the present study. Finally, to make a closure to the mathematical model, the following ideal gas approximation is considered:

$$P = \frac{k}{\bar{m}}(1+\alpha)\rho T \tag{7}$$

where $\bar{m}$ is determined based on the calculated mass fraction of the polycarbonate plasma density to the total mass density during the computation. In this mathematical model, magnetic pinch pressure in the bore is not considered, because it would be negligible compared to the typical range of thermodynamic pressure (10–100 MPa) in the plasma flow. In the present modeling, the vaporization of the fuse wire is ignored, since initial arc establishing process by fuse wire explosion lasts less than 20 μs judging from the measurement of voltage drop across the bore capillary. Also, mass erosion from the electrodes is disregarded due to large aspect ratio of the bore.

2.3. Thermodynamic and transport properties of plasma

Since typical conditions in ETC gun are extremely high pressure and temperature, ablated material is expected to be

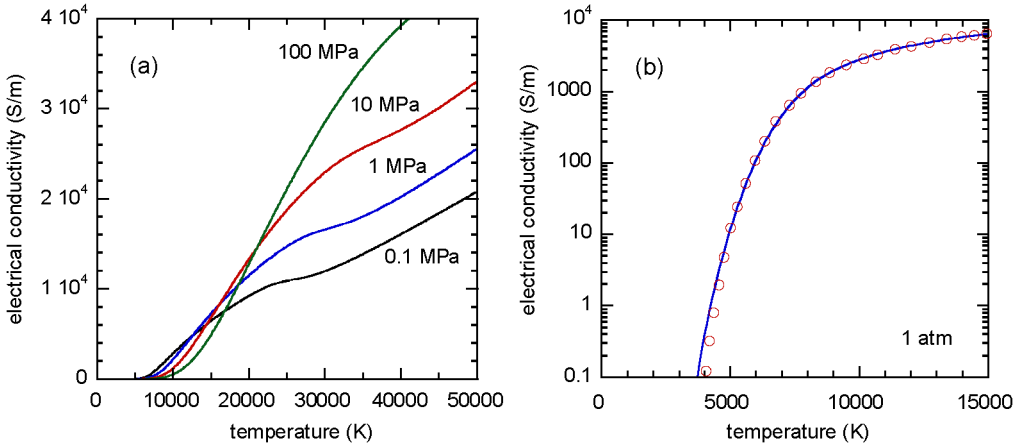

Fig. 3. Electrical conductivity for the polyethylene plasma as a function of temperature and pressure (a); comparison of data at 1 atm (b). Symbols represent the computational results by André and Brunet [15] and solid lines are from present calculations.

fully dissociated into their elemental constituents and partially or fully ionized. Also, at such extreme conditions, plasmas are in local thermodynamic equilibrium, which implies that the composition and the thermodynamic properties of the plasma can be determined by the local state of the plasma. The equilibrium compositions of the plasma are determined by solving the following form of the Saha equation:

$$\frac{n_{i+1}n_e}{n_i} = 2\frac{Q_{i+1}}{Q_i}\left(\frac{2\pi m_e kT}{h^2}\right)^{3/2}\exp\left(-\frac{I_i - \Delta I_i}{kT}\right) \tag{8}$$

The partition functions Q_i can be determined by considering the degeneracy and the energy of electronic excitation level. The term ΔI_i is the correction to the ionization energy of heavy species, I_i, for the nonideal plasma behavior. The degree of plasma nonideality can be quantified as the following nonideality parameter [11]:

$$\gamma = \frac{e_c^2(n_{\text{ion}} + n_e)^{1/3}}{4\pi\varepsilon_0 kT} \tag{9}$$

For the plasma state of present interest (10 000–30 000 K and 10–100 MPa), this parameter is usually found to be well below unity, and the plasma can be considered as weakly nonideal. Therefore, the pressure correction to the ideal gas equation of state is not significant and the above nonideal plasma correction to the plasma properties is sufficient in this study. In fact, André et al. [12] showed that Debye–Hückel or virial corrections to the kinetic pressure yield usually less than three percent difference in their plasma property calculation for the polycarbonate plasma. Note that up to two ionization levels of the atomic heavy species are considered in this study.

For a partially or fully ionized plasma, electrical conductivity is determined based on the electron collisions with both neutral atoms and ions and can be expressed as

$$\sigma = \frac{n_e e_c^2}{m_e(\bar{\nu}_{en} + \bar{\nu}_{ei})} \tag{10}$$

In evaluating $\bar{\nu}_{ei}$, Zollweg and Liebermann model [13] is employed for a correction to traditional Spitzer formula [14] to account for nonideal effect in a dense plasma. Electrical conductivity of the polyethylene plasma is plotted in Fig. 3(a) as a function of temperature and pressure. In Fig. 3(b), present calculation of electrical conductivity at the standard atmospheric pressure is compared with the computation of André and Brunet [15], who included more complex species such as C_2, H_2, CH_2, C_2H, C_2H_2, etc., in their thermodynamic property formulations. Those diatomic and polyatomic species become important at relatively low temperature of less than 5000 K and the comparison shows the discrepancy is noticeable only below 5000 K. Therefore, simplified approach of only including monoatomic species could be acceptable in providing reasonably accurate transport properties to present computations of typical plasma conditions in ETC gun operations. More details on the calculation of thermodynamic and transport properties of plasma vapor in local thermodynamic equilibrium can be found in the works of Raja [11] or Batteh et al. [16].

2.4. Numerical solution procedure

The numerical scheme employed in this article is based on LCPFCT [17] which uses the one-dimensional flux-corrected transport (FCT) algorithm with fourth-order phase accuracy. This scheme is originally developed by Boris [18] and solves the generalized one-dimensional continuity equation in the form of

$$\frac{\partial\phi}{\partial t} + \frac{1}{r^{n-1}}\frac{\partial}{\partial r}\left(r^{n-1}\phi u\right) = \frac{1}{r^{n-1}}\frac{\partial}{\partial r}\left(r^{n-1}D_1\right) + C_2\frac{\partial D_2}{\partial r} + D_3 \tag{11}$$

where ϕ is the generalized conserved quantity such as ρ, ρ_p, ρu_z, and $\rho\varepsilon$, and the terms C_2, D_1, D_2, and D_3 accommodate the source terms. The integer n becomes one for the axial direction here in one-dimensional modeling.

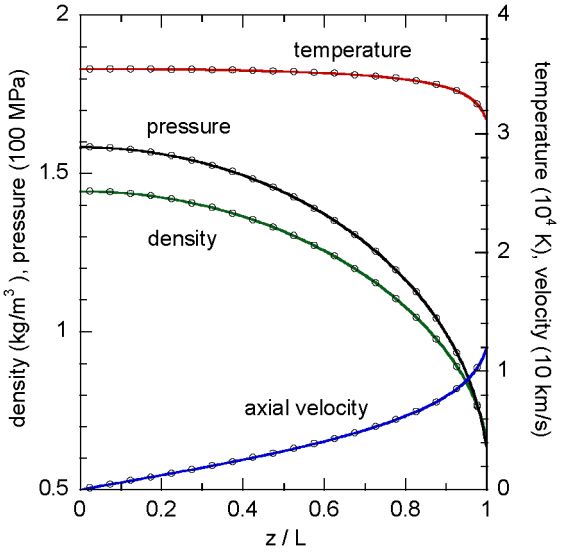

Fig. 4. Axial distribution of plasma flow properties at 450 μs for shot 8.

It is well known that the flow be choked at the open end of the bore, due to the Joule heating from the electrical discharge and the mass ablation from the bore wall, and the flow properties inside the bore become independent of the conditions outside the bore. Therefore, the sonic boundary condition can be applied at the bore exit and the speed of sound in a plasma at the bore exit is approximated under the assumption of isentropic equilibrium flow conditions.

$$c_s = \left(\gamma_{\text{eff}}(1+\alpha)R_h T\right)^{1/2} \tag{12}$$

where R_h is the average gas constant of heavy species. In above equation, using ideal gas approximation, effective specific heat ratio γ_{eff} is evaluated as

$$\gamma_{\text{eff}} = 1 + \frac{P}{\rho e} \tag{13}$$

Imposing sonic condition at the exit could be questionable at an very early stage of plasma discharge. Due to immense energy deposition due to Joule heating, sonic condition could be established right after the start of computation, even though the accuracy may be questionable on that period of time. However, time period for establishing choked exit is estimated to be approximately 20 μs, which could be negligible compared to discharge duration of 1 ms. Additionally, it should be noted that the explosion of wire is the dominant phenomena at the very early stage of discharge and its effects are not included in the present study. At the closed end of the bore, solid wall boundary conditions are imposed such as $u_z = 0$ at $z = 0$. The computations shown in this study were performed on the uniform grid system of 300 grid points between the two ends of the capillary bore. Through a grid resolution study, this grid resolution is found to be sufficient in resolving the axial variation of plasma properties and the comparison with finer grid system will be presented in the next section. Integrating time step

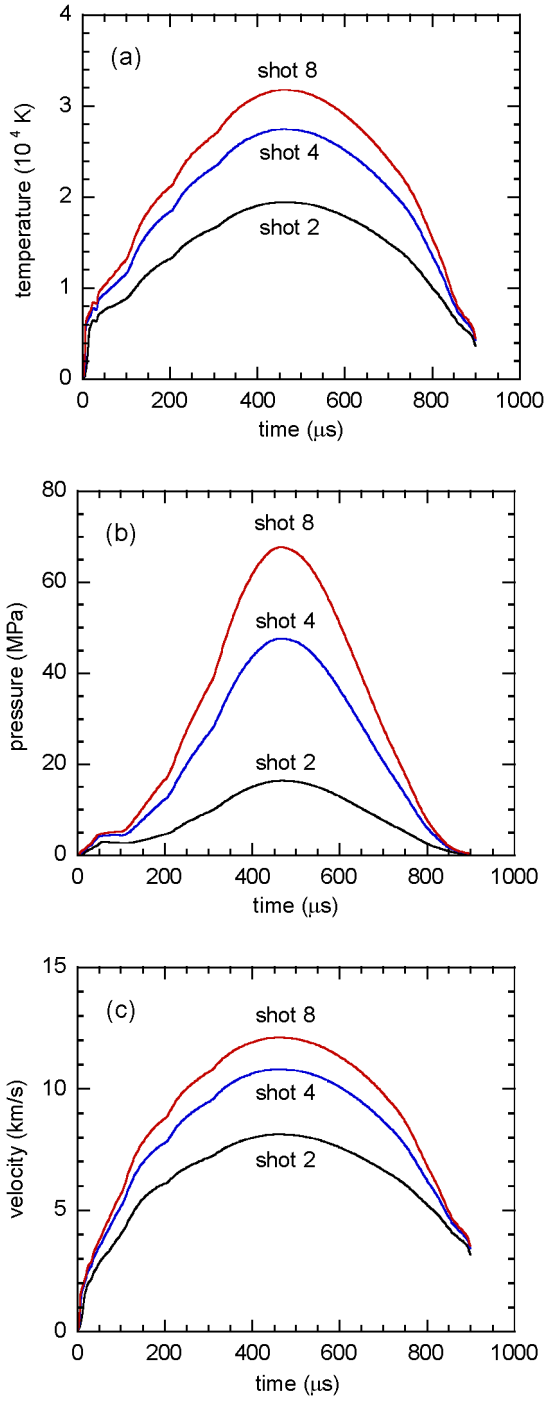

Fig. 5. Plasma discharge conditions at the bore exit. (a) Temperature; (b) pressure; (c) axial velocity.

is determined by the CFL condition with the CFL number of 0.5.

3. Results and discussion

Previously mentioned ETC gun firing of total eight shots are numerically simulated as the experimentally recorded arc current traces are served as the input with given geometry of

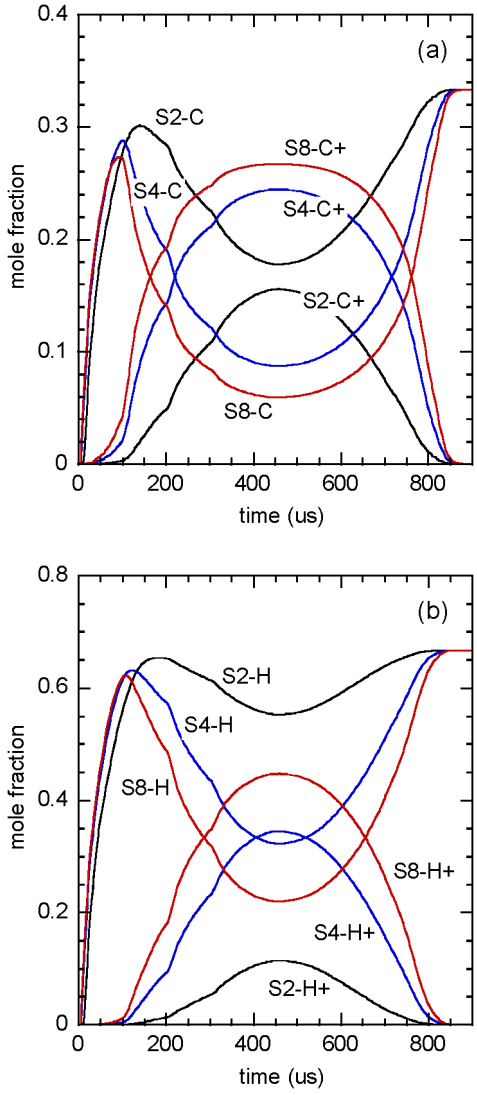

Fig. 6. Temporal variation of species mole fractions at the bore exit for shots 2, 4, and 8. (a) Carbon; (b) hydrogen.

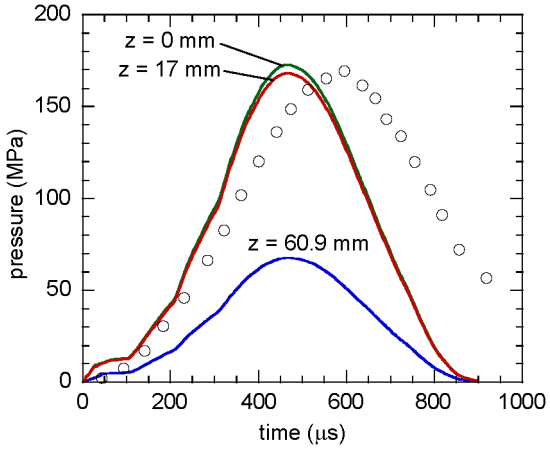

Fig. 7. Pressure evolution at the axial location of $z = 0, 17$, and 60.9 mm for shot 8. Symbols represent the measurements at $z = 17$ mm [4].

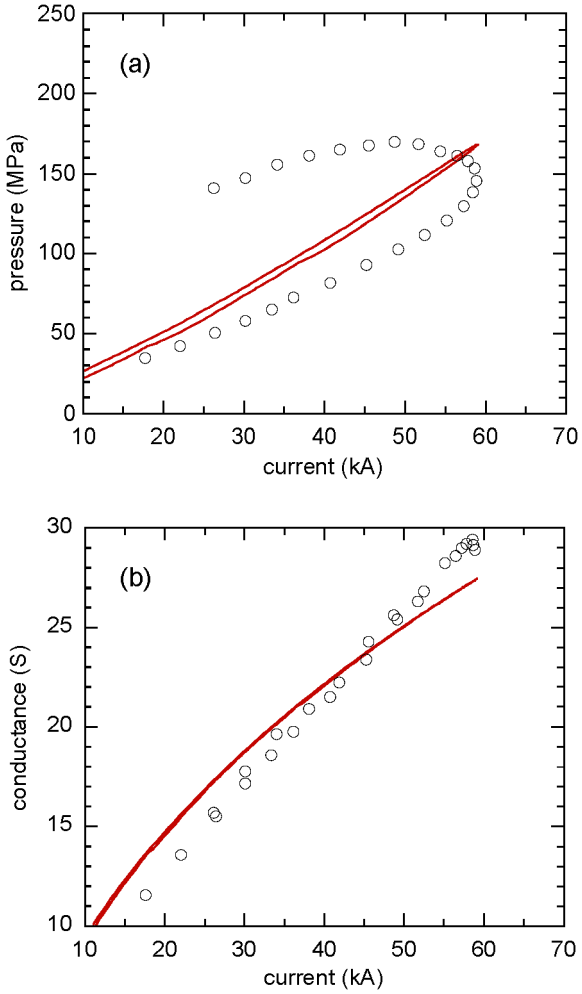

Fig. 8. Temporal variation of (a) pressure at $z = 17$ mm and (b) conductance as a function of current for shot 8. Symbols represent the experimental data [4] and the lines are from present calculations.

the bore. In Fig. 4, axial variation of plasma flow properties at 450 μs is plotted for shot 8. Temperature distribution is nearly constant along the axial direction except the region near the bore exit where temperature exhibits a steep decrease. This trend of small axial temperature variation justifies previously mentioned isothermal models. Plasma pressure and mass density show the monotonic decrease along the axial direction, and maximum pressure at the closed end of bore ($z = 0$) is roughly two times higher than exit bore pressure. The axial velocity increases rapidly along the bore length and the exit plasma velocity is approximately 12 km·s^{-1}. Additionally, in Fig. 4, the computational results using 300 grid points (sold lines) and 600 grid points (symbols) are compared in order to assess the adequacy of the grid resolution and it is found that 300 grid points is sufficient in resolving spatial variation of flow properties.

Fig. 5 shows the temporal evolution of temperature, pressure, and axial velocity at the bore exit for shots 2, 4, and 8 with total energy deposition of 7.3, 21.4, and 47.0 kJ, respectively. For shot 8, the exit conditions at the time of peak current are approximately 68.2 MPa of pressure, 31 740 K

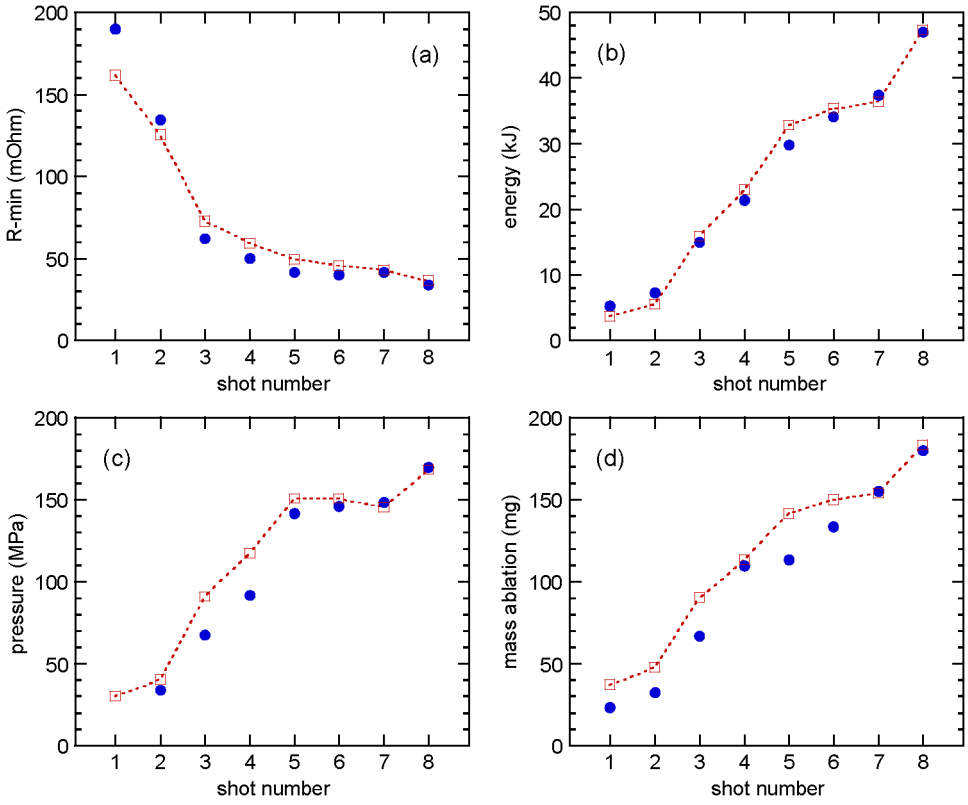

Fig. 9. Comparison with experimental data. (a) Minimum resistance; (b) total deposited energy; (c) maximum pressure at $z = 17$ mm; (d) total mass ablation. Filled symbols represent the experimental data [4] and the dotted lines are from present calculations.

of temperature, and 0.70 kg·m^{-3} of density. Present study includes four molecular species: carbon and hydrogen from bore wall erosion and nitrogen and oxygen from initial quiescent air. Among them, mole fractions of carbon and hydrogen heavy species (C, C^+, H, H^+) at the bore exit are shown in Fig. 6 for shots 2,4, and 8, indicating that level of ionization increases with increasing energy deposition as expected. Degree of ionization of plasma at the bore exit is found to be 0.27, 0.59, and 0.73 for shots 2, 4, and 8, respectively, and plasma is partially ionized for present range of energy deposition. Note that the second level of ionization for carbon species (C^{++}) is negligible for all cases here.

Fig. 7 represents the temporal evolution of the pressure at three axial locations of bore length ($z = 0, 17$, and 60.9 mm), which is compared with the pressure measurement at $z = 17$ mm. While the present calculation agrees well with the measurements for the maximum value of the pressure, the measurements exhibit significant transient effect with the shift of approximately 70 μs compared to the maximum pressure from the calculation. In Fig. 8(a), measurements and the calculations are now compared as a function of arc current to investigate the transient effect on the pressure furthermore. The measurement shows the significant difference of the pressure for the rising or falling current and the pressure evolution with falling current is roughly two times higher than the pressure with rising current. This transient effect can be seen in the computational results, as the pressure with falling current is higher than the pressure with rising current, however the pressure difference is insignificant compared to the trend found in the measurements. While slow response of the pressure transducer might be the reason for this transient effect, the other possible explanations would be two-dimensionality of the plasma flow due to vapor plasma boundary layer on the bore wall or effect of wall heating on bore erosion mechanism. In Fig. 8(b), overall conductance of the plasma flow, which is evaluated by integrating the plasma electrical conductivity over the inner bore volume through the pulse duration, is compared very well with the measurements. Unlike pressure evolution, conductance does not reveal noticeable transient effect and its temporal behavior is predominantly quasi-steady.

Computational results for the rest of the shots are compared with the measurements in four plots of Fig. 9. Minimum plasma arc resistance during the plasma discharge occurs approximately at the time of peak current and it can be easily determined in the measurements by recording the voltage drop across the capillary. As shown in Fig. 9(a), numerically evaluated minimum arc resistance agrees well with measurements for all shots. Agreement on shot 1 of lowest energy deposition is less desirable and it is possibly due to the approximation of not including diatomic and polyatomic species in evaluating thermophysical properties.

Total energy deposition in the capillary is also determined by integrating the Joule heating contribution over the inner bore volume and the entire duration of the firing, and the results show excellent agreement with the experimentally determined values, as can be seen in Fig. 9(b). Despite previously discussed transient effect on the pressure measurements, maximum pressures obtained from the measurements at the axial location of $z = 17$ mm are favorably compared with the calculations in Fig. 9(c). Note that maximum pressures for shots 5, 6, and 7 are fairly unchanged despite the increasing energy deposition. This is due to the enlarging bore diameter as listed in Table 1, and the energy deposition per unit volume is nearly constant among those shots. In comparison of mass ablation from the bore wall in Fig. 9(d), agreement is good but less favorable than previous comparisons. Simulations give excellent prediction on high energy firings (shots 7 and 8), but mass ablation is generally overpredicted in lower energy firings. Modeling of mass ablation from bore wall or electrodes is probably the most difficult challenge and there is clearly a need for more sophisticated model.

4. Conclusions

Pulsed plasma discharge by the electrothermal–chemical gun is numerically investigated using one-dimensional time-dependent gas dynamics simulations. In the mathematical model, Joule heating and the mass ablation are incorporated as well as the evaluation of thermodynamic and transport properties of the weakly non-ideal plasma under the assumption of local thermal equilibrium. The computational results are favorably compared with the measurements of total eight shots of ETC gun firing with different levels of energy deposition ranging from 5.3 to 47 kJ. Deviation factor from the blackbody radiation is set to be 0.85 in the modeling of mass ablation, and the predicted mass ablation agrees well for all the shots. Plasma discharge at the bore exit is found to be partially ionized and the second level of ionization is negligible. Temporal evolution of pressure shows transient effect in the calculations but the effect is minimal compared to the significant transient effect in the pressure measurements. However, the maximum pressure is in good agreement. In contrast, plasma arc resistance exhibits quasi-steady behavior both in the calculations and the measurements.

References

[1] K.J. White, G.L. Katulka, T. Khong, K. Nekula, Plasma characterization for electrothermal-chemical (ETC) gun applications, ARL-TR-1491, 1997.
[2] D.R. Peterson, Electrothermal–chemical synthesis of nanocrystalline ceramics, PhD thesis, The University of Texas at Austin, Austin, TX, 1996.
[3] R.B. Mohanti, J.G. Gilligan, Time-dependent simulation of the plasma discharge in an electrothermal launcher, IEEE Trans. Magn. 29 (1) (1993) 585–590.
[4] J.D. Powell, A.E. Zielinski, Theory and experiment for an ablating-capillary discharge and applications to electrothermal–chemical guns, BRL-TR-3355, 1992.
[5] L.L. Raja, P.L. Varghese, D.E. Wilson, Modeling of the electrogun metal vapor plasma discharge, J. Thermophys. Heat Transfer 11 (3) (1997) 353–360.
[6] J.D. Powell, A.E. Zielinski, Capillary discharge in the electrothermal gun, IEEE Trans. Magn. 29 (1) (1993) 591–596.
[7] D. Zoler, R. Alimi, A proof of the need for consistent treatment in modeling of capillary ablative discharges, J. Phys. D: Appl. Phys. 28 (1995) 1141–1152.
[8] M.F. Zaghloul, M.A. Bourham, J.M. Doster, Semi-analytical modelling and simulation of the evolution and flow of ohmically-heated non-ideal plasmas in electrothermal guns, J. Phys. D: Appl. Phys. 34 (7) (2001) 772–786.
[9] K. Kim, Time-dependent one-dimensional modeling of pulsed plasma discharge in a capillary plasma device, IEEE Trans. Plasma Sci. 31 (4) (2003) 729–735.
[10] J.U. Kim, N.T. Clemens, P.L. Varghese, Experimental study of an underexpanded pulsed plasma jet, AIAA Paper 99-0452, 1999.
[11] L.L. Raja, A theoretical model for the metal vapor plasma discharge of an electrothermal gun, PhD thesis, The University of Texas at Austin, Austin, TX, 1996.
[12] P. André, L. Brunet, E. Duffour, J.M. Lombard, Composition, pressure and thermodynamic properties calculated in plasma formed in insulator vapours of PC and POM at fixed volume, European Phys. J. AP 17 (2002) 53–64.
[13] R.J. Zollweg, R.W. Liebermann, Electrical conductivity of nonideal plasmas, J. Appl. Phys. 62 (9) (1987) 3621–3627.
[14] L. Spitzer, Physics of Fully Ionized Gases, Interscience, New York, 1956.
[15] P. André, L. Brunet, Theoretical computation of the electrical conductivity of thermal plasmas—application to plasma torch design of an electrothermal launcher, IEEE Trans. Plasma Sci. 29 (1) (2001) 19–28.
[16] J. Batteh, J. Powell, D. Sink, L. Thornhill, A methodology for computing thermodynamic and transport properties of plasma mixtures in ETC injectors, IEEE Trans. Magn. 31 (1) (1995) 388–393.
[17] J.P. Boris, A.M. Landsberg, E.S. Oran, J.H. Gardner, LCPFCT—Flux-corrected transport algorithm for solving generalized continuity equations, NRL Report No. 6410-93-7192, 1993.
[18] J.P. Boris, Flux-corrected transport modules for generalized continuity equations, NRL Memorandum Report 3237, 1976.